ELSEVIER

Contents lists available at ScienceDirect

# Composites Part C: Open Access

journal homepage: www.sciencedirect.com/journal/composites-part-c-open-access





# Effective reinforcement of engineered sustainable biochar carbon for 3D printed polypropylene biocomposites

Zaheeruddin Mohammed, Shaik Jeelani, Vijaya Rangari

Department of Materials Science & Engineering, Tuskegee University, Tuskegee, AL 36088, United States of America

#### ARTICLE INFO

# Keywords: Biochar Biocomposite Ultrasonication Carbon 3D printing

#### ABSTRACT

Carbon materials derived from sustainable biomass are widely being used as reinforcement fillers to alleviate the use of fossil fuel derived carbon materials in composites. However, high loading percentages of biochar carbons are required for effective reinforcement, because biochar derived traditionally are of low quality. In current study, high quality biochar was synthesized from sustainable starch based packaging waste using a high temperature/pressure pyrolysis reaction. Thus, obtained biochar was further modified using ultrasonication to reduce the particle sizes and increase active surface area making it more compatible for dispersion and 3D Printing. The BET surface area of ultrasonicated carbon was 185.08 m<sup>2</sup>/g; it was also observed that the modified biochar developed nanoscale morphology due to effect of ultrasound on surface of carbon. XRD and Raman analysis revealed that the carbon obtained was highly graphitized. SEM and TEM micrographs revealed that the carbon obtained has graphitic regions with nano surface morphologies. The modified biochar was used as an effective reinforcement filler with polypropylene polymer at a relatively low loading of 0-1 wt.%. The tensile modulus and strength increased by 34% and 46% respectively with a loading of just 0.75 wt.%. Thermal stability of the composite material also improved by delay of 51° C in onset of decomposition temperature and 40° C in maximum rate of decomposition temperature at 0.75 wt.%. Failure analysis of fractured surface revealed that ultrasonicated biochar was effective in reinforcing the material due to improved available surface area and nanosize defects formed on the surface of biochar carbon.

#### 1. Introduction

Polymer nanocomposites with carbon based reinforcement fillers like fullerene, carbon nanotubes (CNTs), carbon nanofibers (CNFs), graphene nanoplatelets (GNPs) and carbon black (CB) have been extensively used in the recent past to improve the overall properties of composite material like structural integrity, thermal stability, electrical conductivity, electromagnetic shielding, energy storage etc. [1-7]. The primary reason for improvements in the properties of composite is due to inherent properties of carbon-based materials themselves [8]. Carbon based nanomaterials derives its exceptional qualities from its elementary structure called 'graphene', which is considered as the basic building block for all graphitic forms of carbon. Here a single layer of carbon atoms are held together by backbone of overlapping sp2 hybridized bonds. The 2p orbitals that produce the  $\pi$  state bands that delocalize over a sheet of carbon give graphitized carbons their outstanding features. As a result, graphitized carbon are extremely stiff, highly conductive, display high mobility of charge carriers etc.

depending on the degree of graphitization and the way basic graphitized sheets are arranged in the final carbon structure. However, development of such high quality carbon is highly dependent on fossil fuel hydrocarbon gases/liquids like methane, ethylene, acetylene, hexane or propane [9-12] and involves sophisticated processes like chemical vapor deposition (CVD), Physical vapor deposition (PVD), Pulsed laser deposition (PLD), arc discharge, plasma enhanced chemical vapor deposition (P-CVD) etc. [13]. The sustainability of precursors used and synthesis processes involved are the major deciding factors validating the viability of technology particularly for large-scale production of such materials. The precursors involved in these processes are fossil fuel dependent for which there could be crisis in future, and it further escalates environmental concerns like energy crisis, global warming and environmental pollution. In such circumstances, it is highly desirable to develop competitive carbons form sustainable precursor materials while using simple synthesis processes that have potential for large-scale production.

The synthesis of carbon from sustainable biomass-based precursor

E-mail address: vrangari@tuskegee.edu (V. Rangari).

<sup>\*</sup> Corresponding author.

materials, often known as biochar, has attracted the interest of scientists all around the world. Initially, soil remediation, carbon capture, water treatment, and air filtering were among the popular applications for biochar [14-16]. Better competitive biochar for functional applications like composite reinforcement, energy storage, and sensors are being developed in recent years, thanks to a better understanding of carbonaceous structural evolution during biochar production and the development of more controlled processing methods [17-22]. Biochar carbon when used as reinforcement filler with polymer matrix gives excellent mechanical and thermal properties [23-26]. Some biochars have also shown good electromagnetic shielding and electrical conductivity [27, 28]. Particularly when it comes to thermoplastics, biochar has a competitive advantage over other natural fillers, as they are more thermally stable to the heat induced during manufacturing processes like melt blending and extrusion. As mentioned earlier the reinforcement ability of the filler material is directly dependent on inherent properties of filler itself [29]. For this reason, unlike traditional carbon nanomaterials, current biochar is not very effective in improving mechanical, electrical properties of composite at low loading percentages. Thus, there is a need to further modify biochar primarily to improve its inherent mechanical, thermal and electrical properties and eventually make it more competitive for reinforcement of polymers at very low percentages on par with traditional carbon nanomaterials like CNTs and GNPs.

When compared to other polymers, polypropylene (PP) offers a wide range of qualities and is very cost effective, making it a popular material for the development of goods for the automotive, aerospace, electrical, and household appliance industries. However, the PP generated via bulk polymerization methods lacks good mechanical and thermal characteristics [30]. To ameliorate thus attained mechanical and thermal properties, materials researchers have widely used composite approach where reinforcement/filler material is added to improve overall properties of materials. Since there is huge need for the use of sustainable and biodegradable materials, natural fillers have been explored as reinforcement/filler materials. Recently natural fibers like sugar cane bagasse [31,32], ramie [33], hemp [34], yucca aloifolia [35], abaca [36], flax and wool [37], wood, rice husk and wheat husk [38] have been used for reinforcement. In addition to fibers nano/micro size natural filler materials like cellulose and lignin have also been explored as reinforcement fillers for PP [39]. However, carbonaceous materials are still considered relatively effective for reinforcement applications primarily due to their inherent mechanical and thermal properties. Because of high thermal stability compared to natural fillers during extrusion process, high specific strength due to low density, low cost and long-term sustainability, researchers have looked into using biochar as a PP reinforcement. Ikram, S, et al. have used pine wood derived biochar at 500° C to manufacture wood and PP biocomposite [40]. They have investigated effect of factors like coupling agent, biochar particle size, melt flow index and wood content on thermal and mechanical properties of composites prepared via extrusion and injection molding. The most suitable loading for enhanced mechanical and thermal properties was found to be as high as 24 wt.%. It was also observed that high porosity on surface of biochar helps in achieving better mechanical strength, due to infiltration of polymer into pores creating a physical/mechanical bond. As property of biochar is highly dependent on structural evolution and graphitization of biochar during pyrolysis, another study reported by the same group have used wood derived biochar at 900° C. Even though properties of PP/Biochar composite improved with more graphitized biochar the filler percentages were still between 0 and 35 wt.%. With recent technological breakthroughs in additive manufacturing technology, it is now being viewed as a full-scale manufacturing approach rather than only a prototype tool [41]. Due to print head clogging, it has been observed that printing materials with large loadings, particularly with micron-sized particles, is difficult [42]. Particle size, degree of graphitization, uniform dispersion, interface interactions, specific surface area, and other parameters that determine the reinforcing ability of

particulate filler are well recognized based on previous knowledge of small particle polymer composites. Implementing controlled slow rate pyrolysis while boosting graphitization by autogenic pressure at high temperatures is one technique to promote carbonization of biochar [43]. Physical procedures such as ultrasonication [44], ball milling [45], and plasma treatments [46], have been utilized as post-treatment mechanisms to improve desirable attributes such as particle size, specific surface area, dispersion, and interface interactions. Ultrasonic irradiation has proven to be very useful technique to improve material properties through acoustic cavitation, which involves the formation, growth and implosive collapse of bubbles in a liquid medium. High-energy ultrasound can be used to prudently break bigger carbonized biochar into smaller particles by exfoliating graphite planes and splitting them, thus improving the overall graphitized biochar structure [47]. Stankovich et al. [48], observed the exfoliation of graphite oxide into 1 nm thin sheets using ultrasonic irradiation. Here ultrasonication was used as a precursor step to physically exfoliate graphene oxide sheets to be followed by chemical reduction of graphene oxide with hydrazine hydrate.

With increasing environmental concerns recyclability of the material is one of the important aspects to be explored to make the material system truly sustainable. Due to worldwide demand for PP being 17% of total plastic generation and waste generation due to PP being 18% of total waste generation, PP has a huge potential to be recycled [49]. Unfortunately, traditionally at the end of product life most of the waste PP either ends up in landfill or littered into environment due to mismanagement [50]. Mechanical recycling of PP is best way to reduce carbon footprint when compared to other methods like chemical and energy recycling of plastics. Spoerk. M et al. [51] showed that PP can be recycled up to 15 times using extrusion based methods without drastic reduction in tensile and impact strength. In 2018, Woern et al. [52] demonstrated feasibility of PP recycling using additive manufacturing method with slight reduction in mechanical properties when compared with its virgin counterparts. Thus it can be established that PP has potential for recyclability making it a great material choice for sustainable product development.

To our knowledge, this is the first time we have reported the synthesis of highly graphitized carbon from starch-based sustainable packaging waste using a controlled pyrolysis reaction involving high temperature/autogenic pressure, and the biochar produced was then further engineered using ultrasonic irradiation. The resulting biochar carbon was highly graphitic, with increased surface area and smaller particles. The carbon produced in this way was employed as a reinforcement filler in a PP matrix. Addition of ultrasonicated biochar at very low percentage loadings unlike conventional higher biochar loadings proved to be effective in improving mechanical and thermal properties of the biocomposites.

#### 2. Experimental

#### 2.1. Materials and methods

## 2.1.1. Materials

Peanut-shaped loose filler packaging waste(PW) material (Bran Foam Top), made primarily from starch, was procured from Ecolopack (Japan) which came as packaging for scientific equipment. Polypropylene (PP) matrix with isotactic crystalline structure, molecular weight 40,000–100,000, powder diameter of  $\sim\!20~\mu m$  and density between 0.910 and 0.928 g/cm³ was obtained from Chem Point (USA).

#### 2.1.2. Methods

2.1.2.1. Pyrolysis. Approximately 25 gm of packaging waste were ball milled for 3 h using stainless steel canisters and 10 mm steel balls at an 8:1 ball to powder ratio, then sieved through  $45\mu$  mesh to eliminate larger particles and achieve uniform size. The sieved powder was then

put into a Ni-based super alloy reactor (GSL-1100X-RC). The chamber was purged with nitrogen gas for 30 min before to the reaction to remove any trapped oxygen/hydrogen gas. To encourage graphitization, PW powder was pyrolyzed at a rate of 10 °C/min up to 1100 °C and maintained for 3 h under autogenic pressure of 150 bar in a high-pressure/temperature reactor itself. The reactor was allowed to cool down to room temperature after the reaction was completed. The biochar was collected and stored in dry place designated as "packaging waste carbon" (PWC-1100).

2.1.2.2. Ultrasonication. In a glass beaker, 2 gm of pyrolyzed biochar and 200 ml of ethanol were irradiated for 3 h with a high-intensity ultrasonic horn (Sonics vibra cell ultrasound, Model VCX 1500). To avoid temperature rise owing to sonication, an external bath of ice was kept to maintain temperature at 5 °C, and the irradiation was done in pulse mode with 30 s ON/ 5 s OFF at an amplitude of 85 percent. Centrifugation (Allegra 64R, Beckman Coulter) at 10,000 rpm for 20 min at 5 °C was used to collect modified biochar. The supernatant was removed, and the leftover biochar powder was dried for 24 h in a vacuum oven. The modified biochar was collected and stored in dry place designated as "Ultrasonicated packaging waste carbon" (US PWC-1100). A schematic of mechanism behind ultrasonication process is shown in Fig. 1.

2.1.2.3. Composite fabrication. To remove any remnants of entrapped moisture, PP powder was dried in an oven overnight at  $100^{\circ}$  C. PWC-1100 biochar and modified US PWC-1100 biochar were blended in different weight percentages, ranging from 0 to 10% for PWC-1100 biochar and 0 – 1% for modified US PWC-1100 biochar. Loading percentages beyond 1 wt.% were not investigated for US PWC-1000/PP composite as loading beyond this percentage leads to agglomerations in composite due to increased surface area and reduced particle size. Biochar was measured and thoroughly mixed with PP matrix using the manual bag method, then mechanically mixed for 5 min at 600 rpm. At temperature of 230 °C and screw speed of 20 rpm, the mixture was extruded using a single screw extruder (EX2 Flilabot with screw L/D = 12 and pitch ½ inch) (Fig. 1. supplementary material). Filabot pelletizer

was used to pelletize the extruded filaments. The pellets were then extruded again at same conditions in the same extruder just to guarantee homogeneous carbon biochar dispersion in PP and extruded into uniform filaments of diameter  $1.7-1.75~\mathrm{mm}$  (Fig. 2. supplementary material). Schematic of sample preparation procedure is shown in Fig. 2. The filaments were then used to print samples.

2.1.2.4. 3D printing of samples. The extruded filaments were used for 3D printing of specimens using a 3D printer system Hydra16A from Hyrel 3D (GA, USA) along with MK450 hot head which is equipped with high torque stepping motor to assist ease in printing of material. The 3D models of test specimens were designed in Free CAD software and sliced using the Slic3r software. Dog bone (Type 1BA) shaped samples according to standard ISO 527–2 were printed for tensile testing (Fig. 4. Supplementary material). Infill type of 0/90° with 100% fill was used, and objects were printed with two perimeters. The rest of printing parameters were set using a Slic3r software as follows: nozzle diameter 0.6 mm; layer height 0.40 mm; nozzle temperature 210 °C (+10 °C for composite); bed temperature 50 °C. The printing speed was fixed at 50 mm/s. To prevent frequent nozzle clogging the retraction length was reduced to 0.4 mm while retraction speed was changed to 25 mm/s.

#### 2.2. Material characterization

#### 2.2.1. Biochar carbon characterization

Fourier transform infrared-attenuated total reflectance (FTIR-ATR) (Thermo Scientific Nicolet iS5) using 32 averaged scans and 4 cm $^{-1}$  resolutions over a range of 4000–500 cm $^{-1}$ . FTIR studies were conducted to validate complete carbonization of packaging waste. Background spectra were taken in the empty chamber before measurements to eliminate the influence of water moisture and CO<sub>2</sub> in the air. X-ray diffraction (XRD) analysis was performed using a Panalytical Empyrean system with a Cu anode ( $\lambda=1.54187$  Å), at 40 kV, 30 mA, and 1.2 kW. Cu K-beta reducing incident optic with  $1/8^{\circ}$  divergence slit and  $1/2^{\circ}$  antiscatter slit was used. The Pixcel 3D detector was used in scanning line mode. The diffraction data for the biochar sample was collected in the  $2\theta$ 

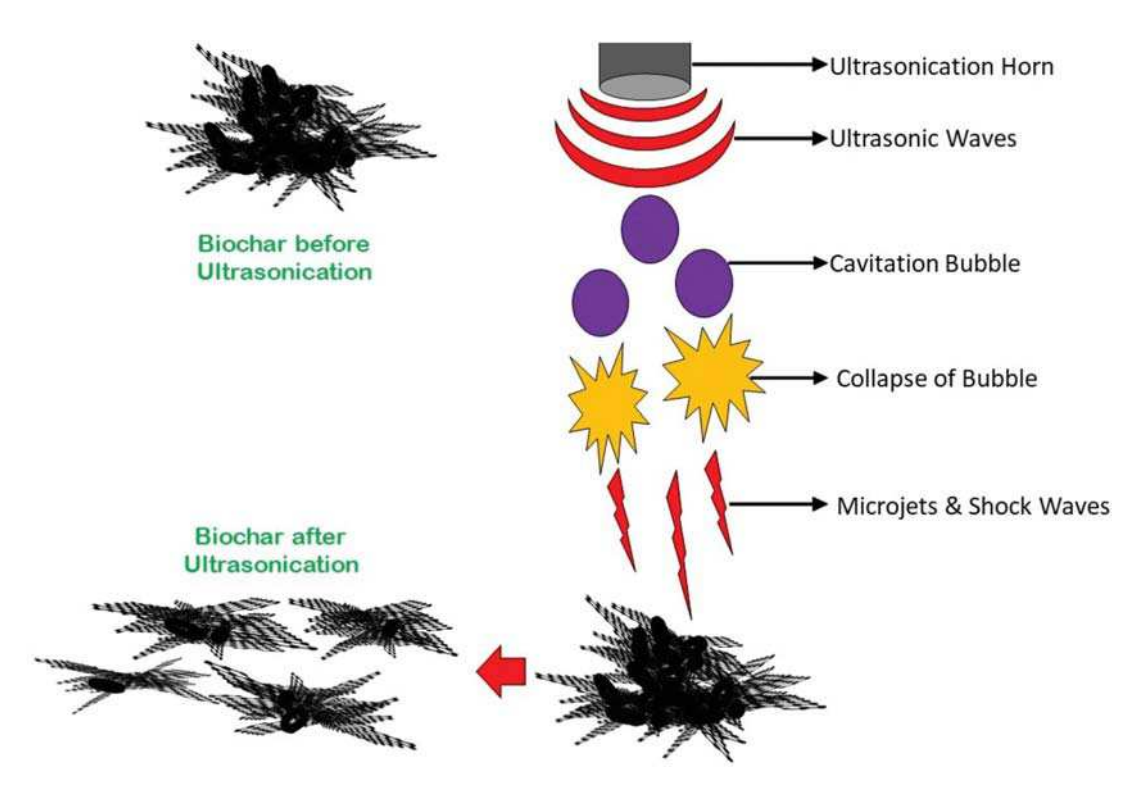


Fig. 1. Schematic diagram showing size reduction mechanism of biochar carbon through ultrasonication.

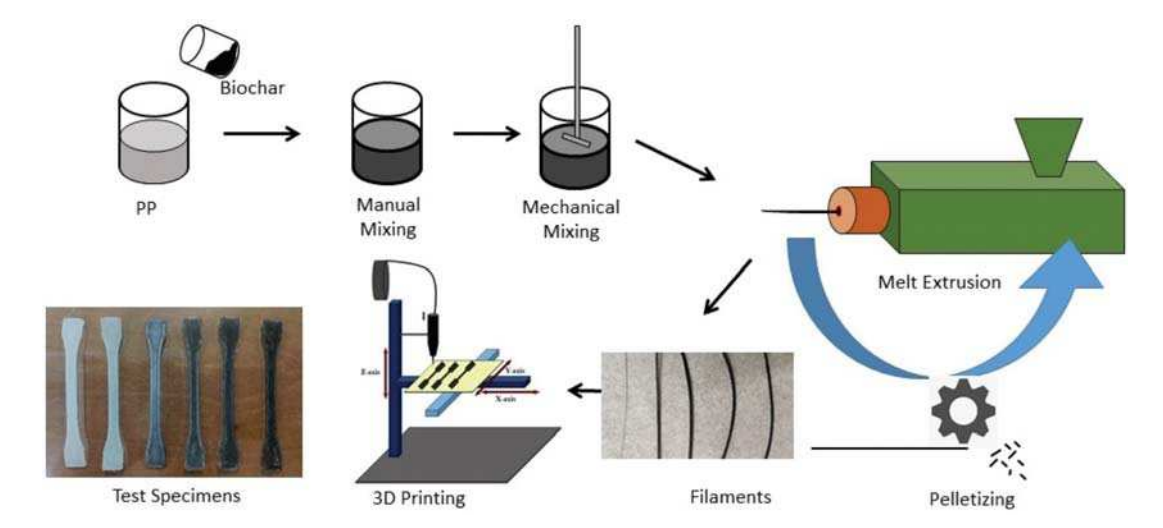


Fig. 2. Composite reinforced with packaging waste carbon fabrication process.

range  $(10-70^\circ)$  at a scan rate of  $2^\circ/\text{min}$ . The Raman spectrum for the biochar was obtained using Thermo Scientific DXR Raman spectroscopy to investigate the graphitization degree and to assess the graphitic and defected carbon. The system is equipped with a laser with an excitation wavelength of 785 nm. The spectrum was obtained in the range of  $500-2500~\text{cm}^{-1}$  using a laser power of 5.0~mW.

Biochar textural properties were investigated using the NOVA2200e (Quantachrome, USA) surface area and pore size analyzer. All samples were vacuum degassed at 300 °C overnight to remove volatiles. Nitrogen adsorption-desorption isotherms were obtained at 77 K and a partial pressure range of 0.05-0.99. Adsorption isotherms were used for the estimation of the BET surface area, volume, and pore size distribution. The Brunauer, Emmett and Teller (BET) surface area was calculated using a multipoint test in a partial pressure range of 0.05-0.3, and the micropore volume was estimated using nonlinear density functional theory (NDLFT). The total pore volume was measured at a partial pressure of 0.99. The surface morphology of the synthesized biochar was investigated using JEOL JSM-7200F field emission scanning electron microscope (FESEM, JEOL USA). Prior to testing the samples were sputter coated with gold/palladium (Au/Pd) for 3 min at 10 mA using Hummer sputter coater to form a conductive surface. Particle sizes were analyzed with the same SEM images using ImageJ software. Microstructure analysis of biochar carbon was done using transmission electron microscope (TEM-Jeol 2010). Carbon was first dispersed in ethanol using ultrasonic bath and then dispensed on Cu grid and air dried. TEM analysis was conducted at an operating voltage of 200 kV.

#### 2.2.2. Composite characterization

A Zwick/Roell Z2.5 Universal Mechanical Testing-Machine with 2.5 kN load cell was used to determine the mechanical properties of the filaments. Tensile test according to ASTM D3379 standard were performed on at least 5 specimens of each type. The testing conditions for the filaments were gauge length of 40 mm, pre-load tension of 0.1 N, and test speed of 0.5 mm/min. Similarly, for tensile testing of 3D printed dogbone shaped specimens the test conditions were gauge length of 20 mm, pre-load tension of 1 N, and test speed of 5 mm/min. The tensile properties as modulus was calculated from linear slope region, tensile strength and elongation at break were obtained with TestXpert data acquisition and analysis software. The machine used crosshead displacement to measure strain values. Influence of individual nanoparticles on thermal stability and residue of the material was investigated using thermogravimetric analysis (TGA) using TA Instruments' Q-500. The equipment was purged with dry nitrogen at 90 mL/min. Samples were scanned from 30 to 800  $^{\circ}\text{C}$  at a ramp rate of 10  $^{\circ}\text{C/min}$ while data for sample weight loss was recorded as function of temperature. Sample weight loss and its derivative weight loss curves were obtained from each test and thermal stability parameters such as onset and decomposition temperatures were recorded along with residue for each sample. DSC was done using non-isothermal mode of scans at 10 °C/min using TA Instruments Q2000 DSC machine. Each sample with weight  $\sim$  6–8 mg was sealed in an aluminum pan and the test was run against an empty reference pan. To eliminate the thermal history of the samples, the neat and BC/PP samples were first heated from (30 to 250 °C) at a heating rate of 10 °C/min and subsequently cooled to 30 °C at the same rate. To avoid any thermal degradation of the samples, the thermal analysis was performed under a nitrogen (N2) atmosphere at a flow rate of 50 cm<sup>3</sup>/min. The melting temperature, crystallization temperature, and enthalpy of melting were analyzed using the TA-Analysis software package based on the second heating and first cooling cycle. To determine the degree of crystallinity of the neat PP and PWC/PP composites, the measured melting enthalpy ( $\Delta H_m$ ) of each sample was compared to the value for 100% crystalline PP ( $\Delta H^0_m$ ). The crystallinity percentage of each sample was calculated by using the total enthalpy method based on following equation.

$$\chi_C(\%) = \frac{\Delta H_m}{(1 - \phi)\Delta H_m^o} \times 100$$

where: (Xc) is the degree of crystallinity, ( $\Delta H_m$ ) is the sample melting enthalpy, ( $\Delta H^0_m$ ) is the enthalpy of melting of 100% crystalline neat PP (207 J/g)  $\phi$  is the weight fraction of BC in the composite. [53]

#### 3. Results and discussion

#### 3.1. Carbon characterization

The FT-IR spectra for the packaging waste powder and pyrolyzed carbon presented in Fig. 3. For PW powder the broad peak around 3300 cm  $^{-1}$  was due to OH stretching, the peak around 2900 cm  $^{-1}$  was due to CH stretching. The transmission hump around 1640 cm  $^{-1}$  was due to OH bending of water, whereas the bands around 1040 and 1100 were due to C—O stretch of polysaccharides kind of material. All these peaks have similar resemblance to that of cellulose-based materials, confirming the major constituent of the packaging waste was starch. [54,55]. However, in case of pyrolyzed carbon it can be seen that there were no significant peaks in the spectra, conforming that the packaging waste is completely aromatized and the functionalities on the surface of carbon are lost making it relatively inert.

XRD graphs of the pyrolzed packaging waste carbon before and after ultrasonication is presented in Fig. 4. a. It can be found that there were

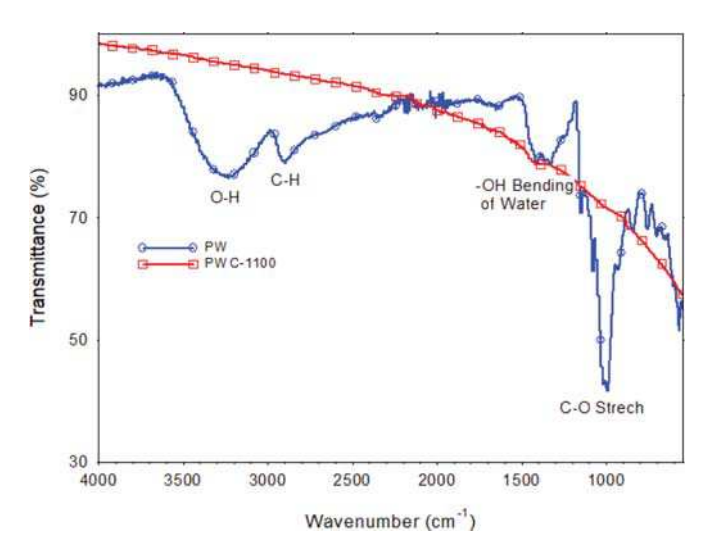


Fig. 3. FT-IR spectra of packaging waste powder and pyrolyzed carbon.

distinct sharp peaks for both carbon around 29° corresponding to (002) plane with an interlayer spacing of 0.30 nm and full width at half maxima of 100% peak is measured as 0.0034 radians, which suggest highly graphitic nature of the carbon. The graphitization of the carbon for this kind of was biochar was mainly due to the pyrolysis process. Slow pyrolysis rate promoted aromatization of the hydrocarbon chains and high temperature/pressure conditions and hold time of 3 h further promoted turbostratic arrangement of the carbon planes; this can be confirmed by (100) peak around 42°. However, the presence of broad peaks around 24° suggests presence of amorphous (early poor crystalline) carbon phase within the material that is typical for biochar materials. The absence of distinct peak due to (101) plane around 45° is an indication that the carbon achieved in this study is not perfectly graphitic in nature. In case of ultrasonicated carbon, there was not much difference in the peaks except that the area of broad peak around 24° corresponding to amorphous region was slightly reduced due to breaking of disordered carbon in the material by action of sonic waves. The intensities of all peaks especially the graphitic peak at 29° corresponding to (002) plane has reduced to some extent suggesting reduction in crystalline quality of planes, this could be mainly due to nanosize defect sites formation on carbon planes due to ultrasonication. The interlayer spacing was 0.30 nm and full width at half maxima of 100% peak measured as 0.0033 radians. Overall XRD results show that the carbon obtained was of high quality when compared with biochar obtained from cellulose based materials in the past [56], and ultrasonication helped in breaking the weaker disordered carbon into smaller carbons with more degree of graphitization however there was also reduced crystallinity due nanopores formed during ultrasonication. To further understand the quality of carbon and effect of ultrasonication, Raman spectroscopy, adsorption test and microstructure analysis was performed.

Raman spectroscopy of synthesized biochar carbon shown in Fig. 4.b revealed that the carbon obtained was of relatively high quality when compared to biochars reported by earlier researchers for similar precursor materials. The characteristic D and G bands, which corresponds to disorder/defect, and graphitic sp<sup>2</sup> hybridized carbon respectively were analyzed in detail. It was revealed that for pyrolyzed carbon (PWC-1100) both distinct peaks of G and D were present confirming the graphitic carbon and polyaromatic hydrocarbons respectively. The G and D band peak for PWC-1100 carbon was obtained around 1600 and 1315 cm<sup>-1</sup> respectively. For ultrasonicated carbon (USPWC-1100) the G and D peaks were found around 1590 and 1310  ${\rm cm}^{-1}$  respectively which were in acceptable range for carbon analysis. ID/IG ratio, which is the ratio of intensities of D and G band, generally used to evaluate degree of disorder in carbonaceous materials was calculated for both the materials. The ID/IG ratio of PWC-1100 was around 1.20 where as for ultrasonicated carbon USPWC-1100 it was around 1.04. The ID/IG ratio of 1.20 is itself a good indication of graphitization with some disorder. Yet, upon ultrasonication the disorder D peak intensity reduced bringing the ID/IG ratio to 1.04 which is indicative of highly graphitized material and is very difficult to achieve for biomass pyrolyzed carbon. It can be also observed from the spectrum that the G band of ultrasonicated carbon is slightly broad when compared to neat carbon; this slight reduction in quality of graphitized carbon was mainly due to defect sites formed in sp<sup>2</sup>-graphitized planes during ulltrasonication that was also observed in XRD analysis. It has to be noted that the increase in overall graphitic nature of carbon in the material is not due to promotion of graphitization, but actually due to reduction in overall disordered carbon found in bigger biochar particles. The mechanism by which ultrasonication reduces the disorder in biochar particles is shown in schematic Fig. 1.

Surface area and textural properties of packaging waste biochar carbon were calculated using nitrogen adsorption and desorption isotherms as shown in Fig. 5(a). It was found that the BET surface area calculated in a partial pressure range of 0.05 to 0.99. was only 2.99  $\rm m^2/g$  for PWC-1100, whereas for ultrasonicated carbon surface area improved to 185.08  $\rm m^2/g$  which is a drastic increase of 60 folds. The main reason for increase in surface area was due to reduction in overall size of the carbon particles and introduction of nano features on the surface of the

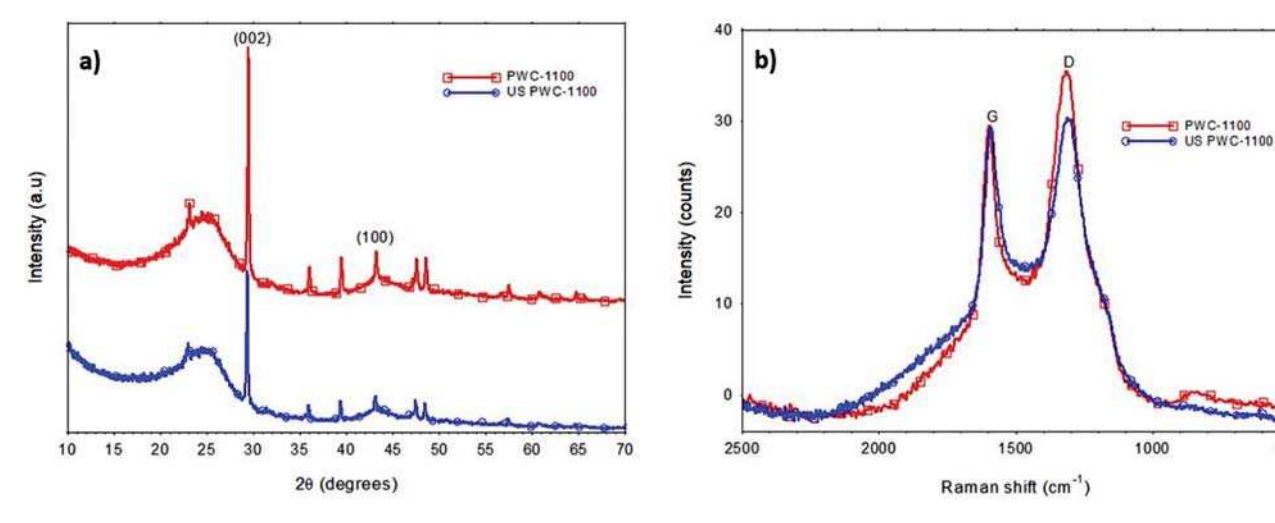


Fig. 4. (a)XRD graph; (b) Raman spectra; of packaging waste derived carbon and ultrasonicated carbon.

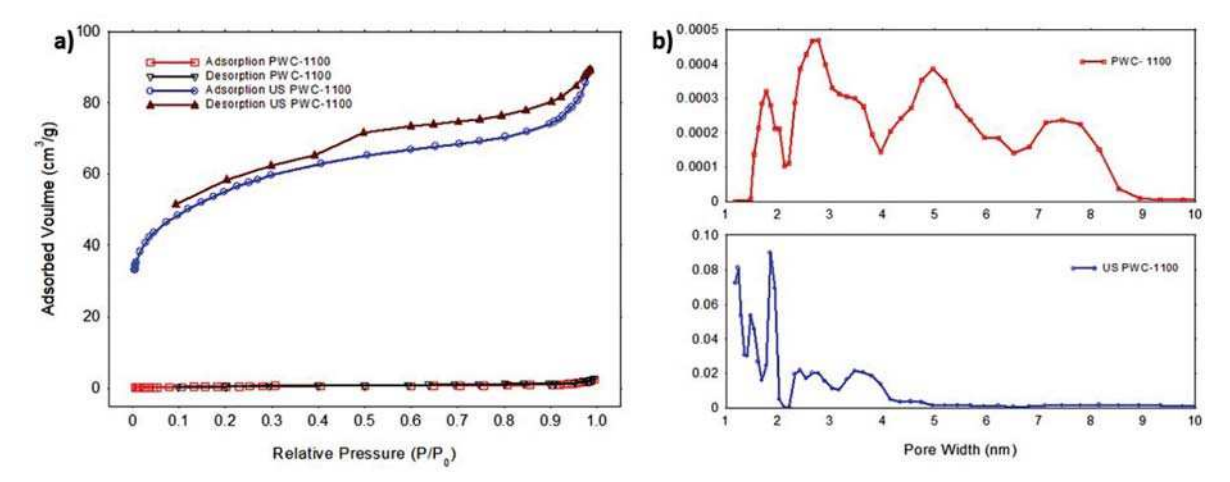


Fig. 5. (a) Nitrogen adsorption-desorption isotherm; (b) Pore size distribution; of packaging waste derived carbon and ultrasonicated carbon.

carbon due to intense shock waves generated during ultrasonication. The average pore size reduced from 6.5471 nm to 2.9931 nm as shown in Fig. 5. b. An interesting observation which can be made is that the pore volume reduced from 0.33 cc/g to 0.122 cc/g, but pore size and pore widths have drastically reduced indicating that the pores were mostly micro size before ultrasonication and after ultrasonication they were mostly *meso* or nanosize pores formed. Table 1 shows a complete comparison of textural properties before and after ultrasonication.

SEM micrographs of packaging waste carbon before and after ultrasonication revealed that the packaging waste biochar originally obtained has particles in the range of few hundreds of micrometers (Fig. 6.a). The particle size analysis of biochar using the SEM images showed that most of the particles ranged between 10 and 60 µm sizes. The average size of the particles were around 36 µm (Fig. 3. Supplementary material). In addition, the carbon surface consisted of many micro size morphologies that might have formed during carbonization process. The morphology of most biochar particles varied between thin sheets and chunks with irregular shapes. Large macropores appeared on the surface of biochar with a size range of  $\sim 1-10 \, \mu m$ . Ultrasonication of carbon helped in breaking of big biochar carbon particles into smaller particles into less than ten micrometer size particles (Fig. 6.b). The surface of the carbon after ultrasonication was relatively smoother when compared to biochar without ultrasonication. However, upon magnification it appeared from the surface that there were some nanosize morphologies introduced due to ultrasonication. The particle size analysis using SEM images revealed that most of the particles were in range of 0.5-2 μm. the average particle size was around 1.9 μm. One interesting observation which can be made here was that even the higher particle sizes were still under 10 µm (Fig. 3. supplementary material). This reduction in sizes of biochar by up to 95% due to ultrasonication will not only help in effective reinforcement at very low loading percentages but also in easy 3D printing of material. To further look at the morphology of carbon at nanoscale TEM analysis was also

TEM micrographs of the biochar carbon revealed that the carbon synthesized was combination of amorphous and crystalline carbon, which was indicated through poorly ordered carbon, and well-ordered

**Table 1**Surface area and textural properties of biochar carbon.

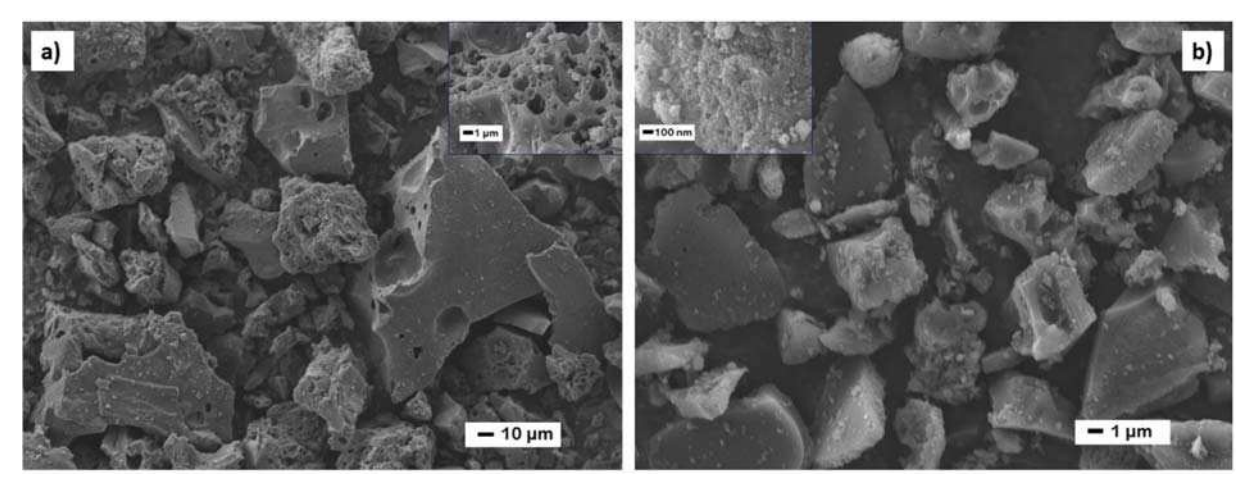
Property	PW carbon	Ultrasonicated PW carbon
BET SSA (m <sup>2</sup> /g)	2.99	185.08
Avg. Pore Size (nm)	6.5471	2.9931
Pore Volume (cc/g)	0.33	0.122
Pore Width (nm)	2.769	1.847
Total Pore Volume (cc/g)	0.0037 (< 260.4 nm)	0.1385 (<137.3 nm)

carbon with well-defined interplanar spacing respectively. It can be observed from TEM micrographs (Fig. 7a and b) that in case of biochar before ultrasonication poorly ordered carbon is more dominant. Whereas, after ultrasonication well-ordered carbon seems to be more dominant. However, it can be also observed that the nanosize morphologies are more observed in ultrasonicated carbon, this could be due to defect sites caused within the planes due to high-energy sonic waves. These TEM micrographs are in good agreement with XRD, Raman and textural results.

#### 3.2. Composite characterization

DSC analysis of biochar carbon reinforced filament composites revealed that the typical endothermic melting was at ~160 °C and exothermic crystallization was around ~115 °C. With addition of biochar, there was a slight increase in melting temperature, due to thermal stability of the filler material. However, melting enthalpy did not increase which might be due to improper interface between polymer and filler. The crystallization temperatures, on the other hand, were pushed to a higher temperature for all samples compared to that of neat PP as shown in Fig. 8.a. This is most probably due to the nucleation effect of the biochar particles in the PP matrix. The biochar particles acted as points from where crystal growth initiated. This effect was not observed predominantly in ultrasonicated carbon composites due to very low loading percentages (Fig. 8.b) .It is interesting to note that the crystallization temperature was higher for biocomposites having higher amount of biochar in it. Although, the difference is not that significant. Thus, increment in the number of biochar particles aids in earlier crystallization of PP. Detailed comparison of various thermal properties of biochar/PP composite is shown in Table 2.

TGA analysis (Fig. 9. a and b) of biochar carbon reinforced filament composites revealed that the thermal properties of all the composites improved when compared with neat PP. With 10 wt.% loading the onset of decomposition was delayed highest by 25° C, where as in case of ultrasonicated carbon thermal properties improved drastically with as little loading as 0.1 wt.%. The best thermal performance was observed in 0.75 wt.% ultrasonicated loaded samples with an effective increase in onset temperature and max rate of decomposition of 51 °C and 40 °C respectively. Such improved thermal stability in ultrasonicated samples is mainly due to the inherent thermal stability of highly crystalline carbon filler material. A detailed comparison of thermal properties like onset of decomposition, max rate of decomposition temperature and residue are tabulated in Table 3. It can be observed that the thermal properties improved for all the composites reinforced with biochar when compared with neat. However, ultrasonicated biochar was more effective in increasing the thermal stability of material system at a very small



 $\textbf{Fig. 6.} \hspace{0.1cm} \textbf{SEM micrographs of (a) packaging waste carbon; (b) ultrasonicated packaging waste carbon.} \\$ 

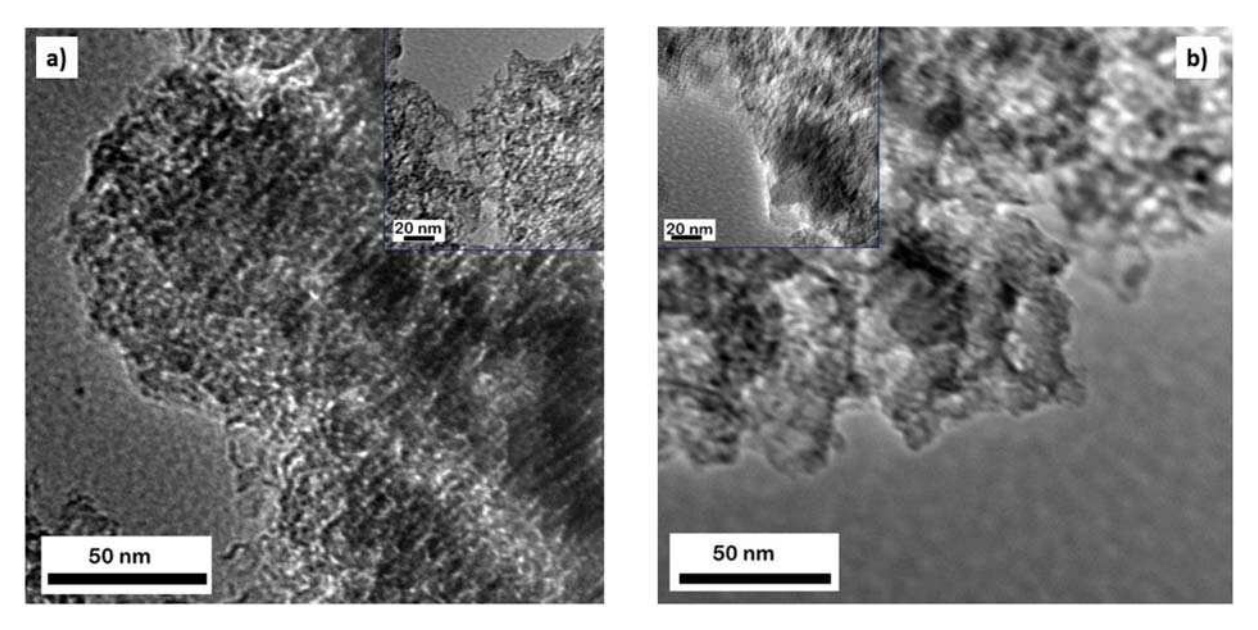


Fig. 7. TEM micrographs of (a) packaging waste carbon; (b) ultrasonicated packaging waste carbon.

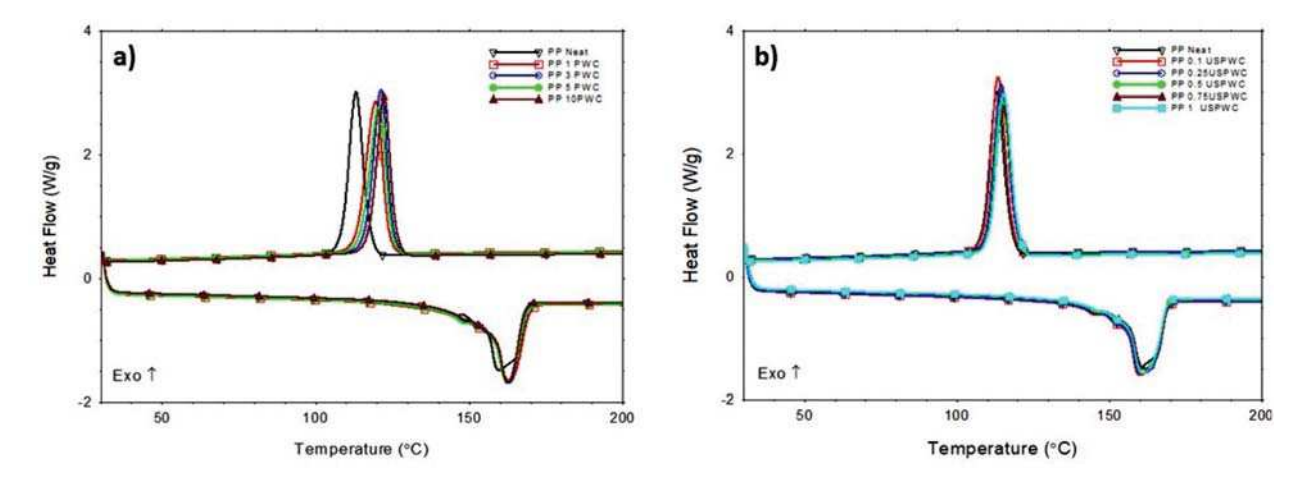


Fig. 8. DSC thermographs of (a) packaging waste carbon reinforced PP composite; (b) ultrasonicated packaging waste carbon reinforced PP composite.

**Table 2**Thermal properties of packaging waste carbon reinforced PP composite filament obtained via DSC.

Composite sample	Tc (°C)	ΔHc (J/g)	Tm ( °C)	ΔHm (J/g)	χc(%)
PP Neat	113.22	98.84	159.72	98.10	47.39
PP 1 PWC	119.59	103.5	163.11	102.40	49.97
PP 3 PWC	121.39	97.81	162.77	96.99	48.30
PP 5 PWC	120.63	98.72	162.47	97.30	49.48
PP 10 PWC	122.29	91.88	162.80	82.64	44.36
PP 0.10 USPWC	113.54	105.2	160.04	99.76	48.24
PP 0.25 USPWC	114.59	103.5	160.97	99.33	48.11
PP 0.50 USPWC	114.83	99.77	161.22	99.07	48.10
PP 0.75 USPWC	115.30	96.43	161.65	97.36	47.39
PP 1.00 USPWC	115.41	100.10	161.13	101.00	49.29

loading percentages. The main reason was due to better inherent thermal properties of filler material itself.

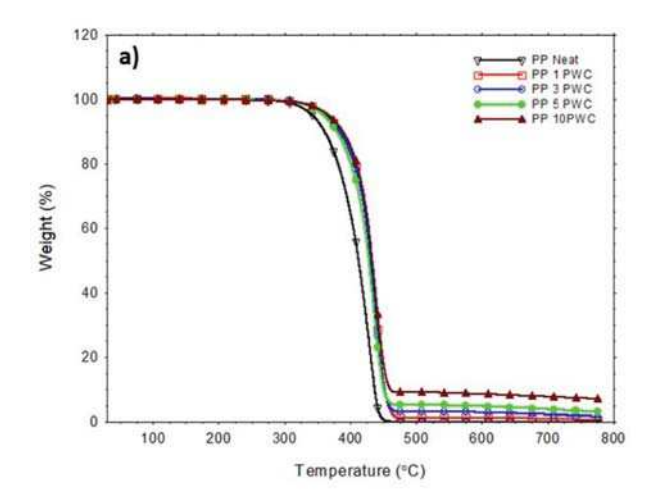
Tensile tests conducted on composite filament samples revealed that biochar filler was effective in increasing the tensile modulus for all the samples. The increase in modulus was mainly due to inherent material property of semi crystalline carbon biochar used as filler. The modulus value increased proportional to the loading percentages. For PWC-1100 reinforced samples the highest modulus was achieved for 10 wt.% loaded samples of 0.71 GPa which was an increase of 86% when compared with neat PP polymer. Tensile strength was recorded highest for 5 wt.% loaded sample at 29.36% which is an improvement of about 35% when compared to neat samples. The primary mechanism of reinforcement in these samples is interlocking of polymer within micro size pores of biochar. The percentage elongation values for all biochar reinforced composites decreased drastically when compared to highly stretchable neat polymer (Fig. 10.a). This behavior was expected, as there is only physical interface between filler and polymer through Vander wall interactions. The ultrasonicated carbon was more effective in increasing strength when loaded with very small loading percentages. At higher loadings, such as 1 wt.% the carbon tends to form agglomerations leading to premature failure as shown in Fig. 10.b. The 0.75 wt.% loaded samples performed best with modulus, strength and elongation values as 0.51 GPa, 31.82 MPa and 17.01% respectively. Which is an improvement of 34% in modulus and 46% in strength. With higher loadings of 1. wt.% modulus improved to 0.58 GPa, but strength and elongation decreased which may be due improper interface or formation agglomerates. Improving the interface between biochar and polymer can be an effective way to improve overall properties of polymer. Detailed comparison of various mechanical properties of biochar/PP composite is shown in Table 4.

Tensile tests conducted on USPWC-1100 reinforced 3D printed dog

bone composite samples revealed that biochar filler was effective in increasing the tensile modulus for all the samples (Table 5). The increase in modulus was again due to inherent material property of semi crystalline carbon biochar used as filler. The modulus value increased proportional to the loading percentages which was the similar trend followed by filament samples also. The tensile strength was better for composite samples when compared to neat, however unlike filament samples there was no particular trend in the strength results. The main reason for very low properties of neat PP samples could be due to dimensional instability after 3D printing of sample particularly due to shrinkage/warpage. Researchers in the past have also reported similar problem with printing of polypropylene material. As polymer melt starts to cool after deposition, the volume of polymer (both free volume between molecular chains and vibrational volume) decreases as long as the temperature is above glass transition, this leads to material shrinkage [57]. This material shrinkage leads to 3D printed layers that lack the ability to adhere to build layers. Hertle et al. [58] proposed that in order to achieve a high interfacial bonding in adjacent layers it should be ensured that the interface between freshly deposited material and previously deposited material should succeed the crystallization temperature up to melting temperature of polymer, in order to enable a short-term melting of crystalline areas of adjacent layers. One way to meet his condition is adding filler materials which can hinder the volumetric change in molecular chains and also prevent rapid crystallization of polymer melt [59]. Hence upon addition of biochar filler material, it was observed that shrinkage gradually reduced proportional

**Table 3**Thermal properties of packaging waste carbon reinforced PP composite filament obtained via TGA.

Composite sample	Decomp onset temp ( °C)	Max rate of decomp temp ( $^{\circ}$ C)	% residue @ 750 °C
PP Neat	342.39	428.59	0.04
PP 1 PWC	363.66	439.66	0.74
PP 3 PWC	363.98	436.58	1.85
PP 5 PWC	359.86	436.53	3.23
PP 10 PWC	367.12	439.95	7.21
PP 0.10 USPWC	361.18	443.71	0.09
PP 0.25 USPWC	380.16	467.11	0.15
PP 0.50 USPWC	385.95	464.35	0.16
PP 0.75 USPWC	393.83	469.06	0.19
PP 1.00 USPWC	392.19	468.63	0.31



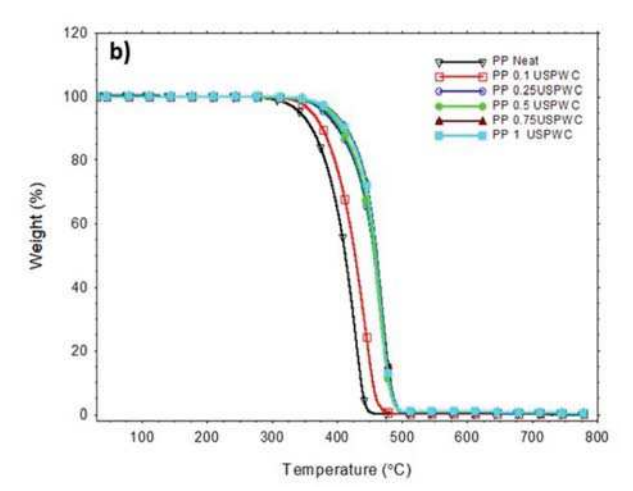


Fig. 9. TGA thermographs of (a) packaging waste carbon reinforced PP composite; (b) ultrasonicated packaging waste carbon reinforced PP composite.

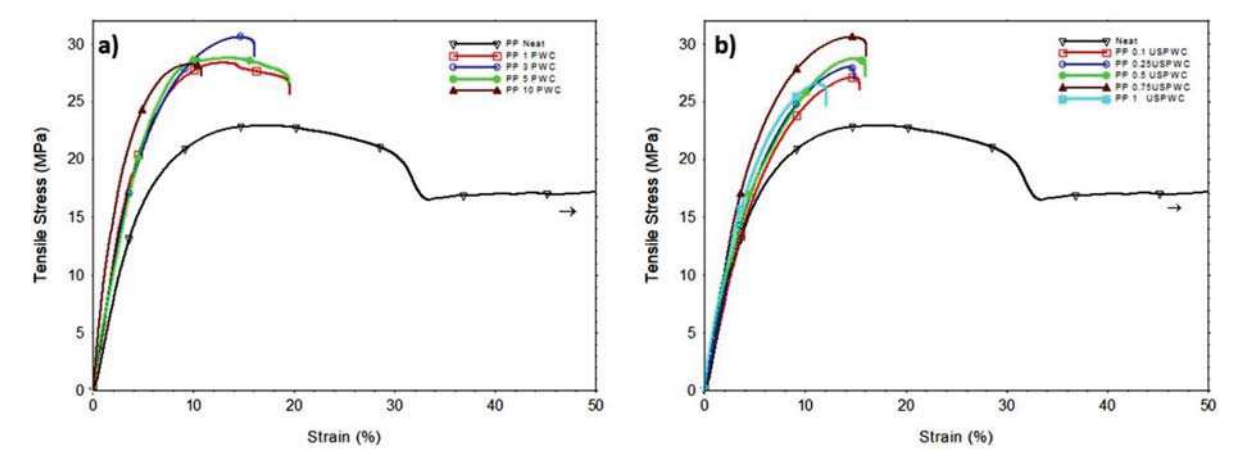


Fig. 10. Stress-strain graphs of (a) packaging waste carbon reinforced PP composite; (b) ultrasonicated packaging waste carbon reinforced PP composite.

Table 4

Mechanical properties of packaging waste carbon reinforced PP composite filament

Sample	Young's modulus (GPa)	Tensile strength (MPa)	Elongation at break (%)
PP Neat	$0.38\pm0.02$	$21.73\pm1.22$	$212.54 \pm 17.23$
PP 1 PWC	$0.50\pm0.05$	$28.14 \pm 5.95$	$21.25\pm3.24$
PP 3 PWC	$0.53\pm0.03$	$31.15\pm3.59$	$18.32\pm3.29$
PP 5 PWC	$0.58\pm0.09$	$29.36\pm4.32$	$20.71 \pm 4.38$
PP 10 PWC	$0.71\pm0.10$	$28.09\pm3.31$	$10.58\pm2.35$
PP 0.10	$0.46\pm0.04$	$26.62\pm2.36$	$16.35\pm5.36$
USPWC			
PP 0.25	$0.48\pm0.03$	$27.21\pm1.24$	$16.06\pm2.32$
USPWC			
PP 0.50	$0.50\pm0.01$	$28.32\pm2.36$	$16.98\pm1.54$
USPWC			
PP 0.75	$0.51\pm0.01$	$31.82\pm0.32$	$17.01 \pm 1.67$
USPWC			
PP 1.00	$0.58\pm0.04$	$26.59\pm2.47$	$12.27\pm1.98$
USPWC			

 $\begin{tabular}{ll} \textbf{Table 5} \\ \textbf{Mechanical properties of packaging waste carbon reinforced PP 3D printed composite.} \\ \end{tabular}$ 

Sample	Young's modulus (GPa)	Tensile strength (MPa)	Elongation at break (%)
PP Neat PP 0.10 USPWC	$\begin{array}{c} 0.041 \pm 0.007 \\ 0.069 \pm 0.003 \end{array}$	$5.01 \pm 1.59 \\ 10.80 \pm 4.66$	$11.02 \pm 2.55 \\ 12.68 \pm 3.98$
PP 0.25 USPWC	$0.090 \pm 0.011$	$18.70\pm6.16$	$13.01\pm2.73$
PP 0.50 USPWC	$0.111 \pm 0.010$	$16.73\pm2.56$	$15.18\pm3.97$
PP 0.75 USPWC	$0.115\pm0.004$	$13.01\pm6.32$	$9.49 \pm 0.06$
PP 1.00 USPWC	$0.128\pm0.002$	$26.03\pm3.32$	$22.11\pm1.43$

to loading percentages, eventually leading to increased mechanical properties. However, it can be observed that the modulus and strength properties of 3D printed parts did not follow any particular trend as in the case of filament samples. This might be due to higher inconsistency in 3D printed samples, which are more heterogeneous and erratic when compared to extruded filaments or injection molded parts. With appropriate process improvements methods and optimization better 3D printed samples with superior properties, reflecting similar trend of filament samples could be fabricated.

Failure analysis of failed samples (Fig. 6. Supplementary Material)

using SEM microscopy revealed that there was little or no resistance to failure of neat samples except for plasticization of overall failure zone as shown in Fig. 11.a. This behavior was due to low load carrying capacity of polymer by itself. The biochar carbon had micropores which was mainly responsible for mechanical interlocking of polymer and matrix as shown Fig. 11. c. In case of biochar reinforced composite, especially the ultrasonicated biochar was effective in reinforcing the material offering good resistance to failure (Fig. 11.b) thus improving the overall mechanical properties. It was also observed that biochar could be seen embedded in the polymer matrix but the failed side was smooth as shown in Fig. 11.d. suggesting lack of proper interface between filler and matrix. This lack of proper interface could be the main reason for drastic drop in elongation of samples.

#### 4. Conclusions

From this study, it can be concluded that high quality semicrystalline biochar carbon can be synthesized from biomass material such as starch based packaging waste thus mitigating the need for synthesizing of carbon nanomaterials from fossil fuel based sources. The quality of the carbon can be further improved using simple ultrasonication method for effective reinforcement and to make it compatible with 3D printing process. Ultrasonication not only reduces the particle size of the carbon but also reduces the overall content of amorphous carbon in the biochar. The surface area can be drastically improved and a more thermally stable material can be developed. The thermal and mechanical properties of the composite material improved, the main reason for such improvements is due to improved quality of filler material and better interaction between polymer and filler material due to enhanced surface area and formation of nanosize defects on the carbon surface. Thermal properties of biochar reinforced composites was best for 10 wt.% loaded samples with initial decomposition at 367.12 °C when compared to 342 °C of neat. In case of ultrasonicated biochar reinforced composites 0.75 wt.% loaded samples performed best with initial decomposition at 393.83 °C with improvement of 51 °C when compared to neat samples. For biochar reinforced composites 5 wt.% loaded samples showed the best mechanical strength of 29.36 MPa which was an improvement of 35%. For ultrasonicated biochar carbon reinforced composites a small loading of just 0.75 wt.% was effective in increasing the strength to 31.82 MPa which is an improvement of 46.33%. Ultrasonicated biochar filler helped in easy printing of samples without clogging the printer head. Failure analysis showed that there was lack of proper interface between filler and polymer matrix, which was reason for reduced elongation when compared to neat samples. The 3D printed samples showed similar trends for tensile modulus; however, tensile strength values did not follow any trend. This could be due to inconsistency in print quality of samples. In conclusion, ultrasonication

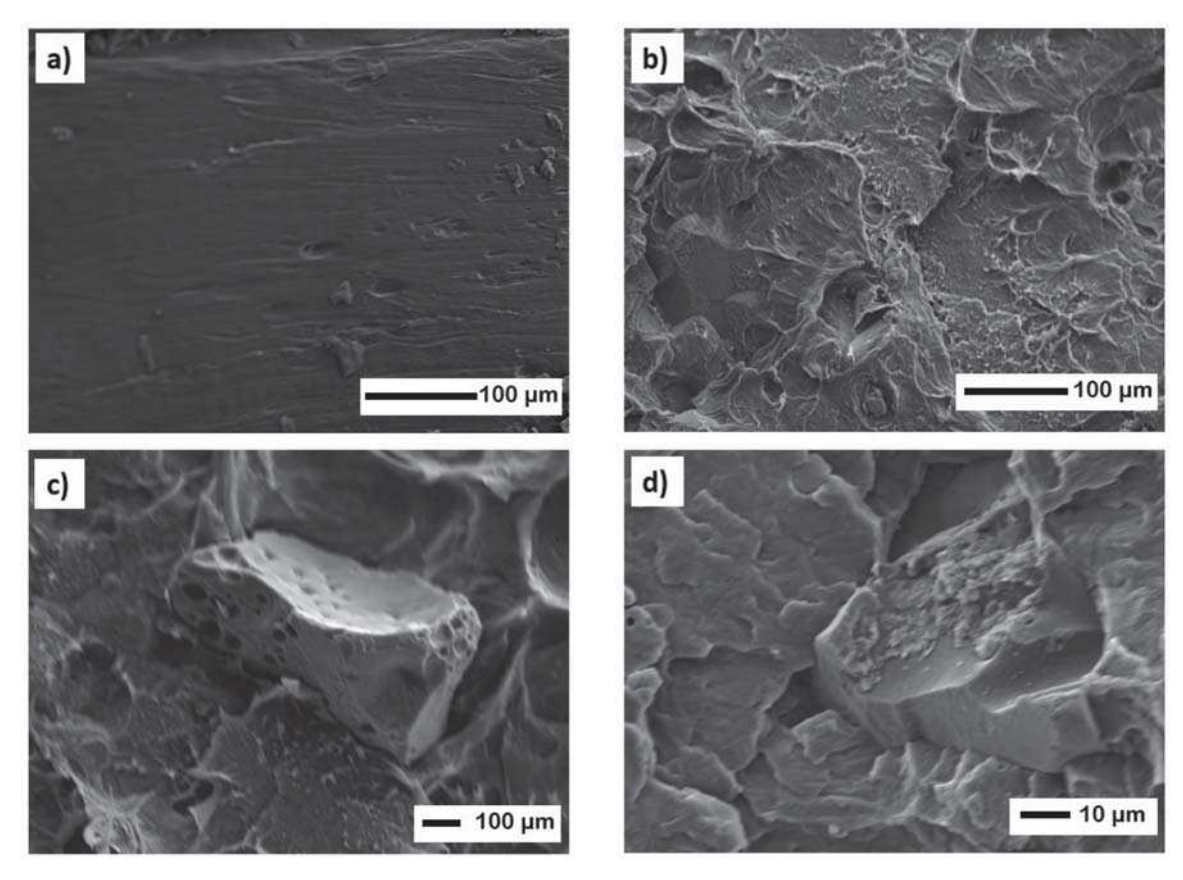


Fig. 11. Failure surface SEM micrographs of (a) Neat PP; (b, d) ultrasonicated packaging waste carbon reinforced PP composite; (c) Packaging waste carbon reinforced PP composite.

of biochar relatively improved the reinforcing ability at very low loading percentages thus making the material more appropriate for 3D printing and improving the overall properties of composites. By optimizing the print parameters and achieving dimensional stability better 3D printed samples with improved properties can be attained.

#### 5. CRediT authorship contribution statement

Zaheeruddin Mohammed: Methodology, Investigation, Data curation, Formal analysis, writing – original draft, Writing – Review and Editing. Shaik Jeelani: Supervision. Vijaya Rangari: Conceptualization, Supervision, Writing- review & editing, Funding acquisition.

## **Declaration of Competing Interest**

The authors declare that they have no known competing financial interests or personal relationships that could have appeared to influence the work reported in this paper.

#### Acknowledgement

The authors acknowledge the financial support of NSF-AL-EPSCoR #1655280, GRSP-Alabama EPSCoR, NSF-CREST#1735971, and NSF-MRI Award #1531934.

#### Supplementary materials

Supplementary material associated with this article can be found, in the online version, at doi:10.1016/j.jcomc.2021.100221.

#### References

- S. Liu, V.S. Chevali, Z. Xu, D. Hui, H. Wang, A review of extending performance of epoxy resins using carbon nanomaterials, Compos. Part B Eng. 136 (2018) 197–214, https://doi.org/10.1016/j.compositesb.2017.08.020.
- [2] Z. Gao, J. Zhu, S. Rajabpour, K. Joshi, M. Kowalik, B. Croom, et al., Graphene reinforced carbon fibers, Sci. Adv. 6 (2020) 1–11, https://doi.org/10.1126/sciadv. aaz4191.
- [3] L. Feng, Y. Zuo, X. He, X. Hou, Q. Fu, H. Li, et al., Development of light cellular carbon nanotube@graphene/carbon nanocomposites with effective mechanical and EMI shielding performance, Carbon N. Y. 168 (2020) 719–731, https://doi. org/10.1016/j.carbon.2020.07.032.
- [4] Z. Mohammed, A. Tcherbi-Narteh, S. Jeelani, Effect of graphene nanoplatelets and montmorillonite nanoclay on mechanical and thermal properties of polymer nanocomposites and carbon fiber reinforced composites, SN Appl. Sci. (2020) 2, https://doi.org/10.1007/s42452-020-03780-1.
- [5] M. Tabandeh-Khorshid, Ajay Kumar, E. Omrani, C. Kim, P. Rohatgi, Synthesis, characterization, and properties of graphene reinforced metal-matrix nanocomposites, Compos. Part B Eng. 183 (2020), 107664, https://doi.org/10.1016/j.compositesb.2019.107664.
- [6] B.G. Compton, N.S. Hmeidat, R.C. Pack, M.F. Heres, J.R. Sangoro, Electrical and mechanical properties of 3D-printed graphene-reinforced epoxy, Jom 70 (2018) 292–297, https://doi.org/10.1007/s11837-017-2707-x.
- [7] S. Zhao, Z. Zhao, Z. Yang, L.L. Ke, S. Kitipornchai, J. Yang, Functionally graded graphene reinforced composite structures: a review, Eng. Struct. 210 (2020), 110339, https://doi.org/10.1016/j.engstruct.2020.110339.
- [8] X. Zhang, N. Zhao, C. He, The superior mechanical and physical properties of nanocarbon reinforced bulk composites achieved by architecture design – a review, Prog. Mater. Sci. 113 (2020), 100672, https://doi.org/10.1016/j. pmatsci.2020.100672.
- [9] D. Ponnamma, Y. Yin, N. Salim, J. Parameswaranpillai, S. Thomas, N. Hameed, Recent progress and multifunctional applications of 3D printed graphene nanocomposites, Compos. Part B Eng. 204 (2021), 108493, https://doi.org/ 10.1016/j.compositesb.2020.108493.
- [10] D. Kuang, L. Hou, S. Wang, H. Luo, L. Deng, J.L. Mead, et al., Large-scale synthesis and outstanding microwave absorption properties of carbon nanotubes coated by extremely small FeCo-C core-shell nanoparticles, Carbon N. Y. 153 (2019) 52–61, https://doi.org/10.1016/j.carbon.2019.06.105.
- [11] L. Lin, H. Peng, Z. Liu, Synthesis challenges for graphene industry, Nat. Mater. 18 (2019) 520–524, https://doi.org/10.1038/s41563-019-0341-4.

- [12] F. Liu, C. Wang, X. Sui, M.A. Riaz, M. Xu, L. Wei, et al., Synthesis of graphene materials by electrochemical exfoliation: recent progress and future potential, Carbon Energy 1 (2019) 173–199, https://doi.org/10.1002/cey2.14.
- [13] D.X. Luong, K.V. Bets, W.A. Algozeeb, M.G. Stanford, C. Kittrell, W. Chen, et al., Gram-scale bottom-up flash graphene synthesis, Nature 577 (2020) 647–651, https://doi.org/10.1038/s41586-020-1938-0.
- [14] N. Cheng, B. Wang, P. Wu, X. Lee, Y. Xing, M. Chen, et al., Adsorption of emerging contaminants from water and wastewater by modified biochar: a review, Environ. Pollut. 273 (2021), 116448, https://doi.org/10.1016/j.envpol.2021.116448.
- [15] J. Liu, B. Jiang, J. Shen, X. Zhu, W. Yi, Y. Li, et al., Contrasting effects of straw and straw-derived biochar applications on soil carbon accumulation and nitrogen use efficiency in double-rice cropping systems, Agric. Ecosyst. Environ. 311 (2021), 107286, https://doi.org/10.1016/j.agee.2020.107286.
- [16] F. Yang, C. Wang, H. Sun, A comprehensive review of biochar-derived dissolved matters in biochar application: production, characteristics, and potential environmental effects and mechanisms, J. Environ. Chem. Eng. 9 (2021), 105258, https://doi.org/10.1016/j.jece.2021.105258.
- [17] D.G. Atinafu, S. Wi, B.Y. Yun, S. Kim, Engineering biochar with multiwalled carbon nanotube for efficient phase change material encapsulation and thermal energy storage, Energy 216 (2021), 119294, https://doi.org/10.1016/j. energy 2020 119294
- [18] J. Liu, H. Ke, K. Zhong, X. He, X. Xue, L. Wang, et al., Higher activity leading to higher disorder: a case of four light hydrocarbons to variable morphological carbonaceous materials by pyrolysis, J. Phys. Chem. C 122 (2018) 29516–29525, https://doi.org/10.1021/acs.jpcc.8b07762.
- [19] W.J. Liu, H. Jiang, H.Q. Yu, Emerging applications of biochar-based materials for energy storage and conversion, Energy Environ. Sci. 12 (2019) 1751–1779, https://doi.org/10.1039/c9ee00206e.
- [20] B. Wang, B. Gao, J. Fang, Recent advances in engineered biochar productions and applications, Crit. Rev. Environ. Sci. Technol. 47 (2017) 2158–2207, https://doi. org/10.1080/10643389.2017.1418580.
- [21] H. Bamdad, S. Papari, S. MacQuarrie, K. Hawboldt, Study of surface heterogeneity and nitrogen functionalizing of biochars: molecular modeling approach, Carbon N. Y. 171 (2021) 161–170, https://doi.org/10.1016/j.carbon.2020.08.062.
- [22] M. Idrees, S. Ahmed, Z. Mohammed, N.S. Korivi, V. Rangari, 3D printed supercapacitor using porous carbon derived from packaging waste, Addit. Manuf. 36 (2020), 101525, https://doi.org/10.1016/j.addma.2020.101525.
- [23] R.K. Dahal, B. Acharya, G. Saha, R. Bissessur, A. Dutta, A. Farooque, Biochar as a filler in glassfiber reinforced composites: experimental study of thermal and mechanical properties, Compos. Part B Eng. 175 (2019), 107169, https://doi.org/ 10.1016/j.compositesb.2019.107169.
- [24] D. Matykiewicz, Biochar as an effective filler of carbon fiber reinforced bio-epoxy composites, Processes 8 (2020) 1–13, https://doi.org/10.3390/pr8060724.
- [25] Q. Zhang, M.U. Khan, X. Lin, H. Cai, H. Lei, Temperature varied biochar as a reinforcing filler for high-density polyethylene composites, Compos. Part B Eng. 175 (2019), 107151, https://doi.org/10.1016/j.compositesb.2019.107151.
- [26] N. Nan, D.B. DeVallance, X. Xie, J. Wang, The effect of bio-carbon addition on the electrical, mechanical, and thermal properties of polyvinyl alcohol/biochar composites, J. Compos. Mater. 50 (2016) 1161–1168, https://doi.org/10.1177/ 0021998315589770.
- [27] A. Noori, M. Bartoli, A. Frache, E. Piatti, M. Giorcelli, A. Tagliaferro, Development of pressure-responsive polypropylene and biochar-based materials, Micromachines (Basel) 11 (2020) 1–12, https://doi.org/10.3390/MI11040339.
- [28] S. Li, A. Huang, Y.J. Chen, D. Li, L.S. Turng, Highly filled biochar/ultra-high molecular weight polyethylene/linear low density polyethylene composites for high-performance electromagnetic interference shielding, Compos. Part B Eng. 153 (2018) 277–284, https://doi.org/10.1016/j.compositesb.2018.07.049.
- [29] O. Das, A.K. Sarmah, D. Bhattacharyya, Structure-mechanics property relationship of waste derived biochars, Sci. Total Environ. 538 (2015) 611–620, https://doi. org/10.1016/j.scitotenv.2015.08.073.
- [30] K. Kalaitzidou, H. Fukushima, L.T. Drzal, A new compounding method for exfoliated graphite-polypropylene nanocomposites with enhanced flexural properties and lower percolation threshold, Compos. Sci. Technol. 67 (2007) 2045–2051, https://doi.org/10.1016/j.compscitech.2006.11.014.
- [31] M. Kumar, A. Singhal, S. Singh, I. Singh, A recyclability study of bagasse fiber reinforced polypropylene composites, Polym. Degrad. Stab. 152 (2018) 272–279, https://doi.org/10.1016/j.polymdegradstab.2018.05.001.
- [32] D.R. Mulinari, P. Cipriano J de, M.R. Capri, A.T. Brandão, Influence of surgarcane bagasse fibers with modified surface on polypropylene composites, J. Nat. Fibers 15 (2018) 174–182, https://doi.org/10.1080/15440478.2016.1266294.
- [33] C.Y. Dang, X.J. Shen, H.J. Nie, S. Yang, J.X. Shen, X.H. Yang, et al., Enhanced interlaminar shear strength of ramie fiber/polypropylene composites by optimal combination of graphene oxide size and content, Compos. Part B Eng. 168 (2019) 488–495, https://doi.org/10.1016/j.compositesb.2019.03.080.
- [34] T. Sullins, S. Pillay, A. Komus, H. Ning, Hemp fiber reinforced polypropylene composites: the effects of material treatments, Compos. Part B Eng. 114 (2017) 15–22, https://doi.org/10.1016/j.compositesb.2017.02.001.
- [35] H.M. Nascimento, D.C.T. Granzotto, E. Radovanovic, S.L. Fávaro, Obtention and characterization of polypropylene composites reinforced with new natural fibers from Yucca aloifolia L, Compos. Part B Eng. (2021) 227, https://doi.org/10.1016/ j.compositesb.2021.109414.
- [36] R. Punyamurthy, D. Sampathkumar, Mechanical properties of abaca fiber reinforced polypropylene composites: effect of chemical treatment by

- benzenediazonium chloride, J. King Saud. Univ. Eng. Sci. 29 (2017) 289–294, https://doi.org/10.1016/j.jksues.2015.10.004.
- [37] N.K. Kim, R.J.T. Lin, D. Bhattacharyya, Flammability and mechanical behaviour of polypropylene composites filled with cellulose and protein based fibres: a comparative study, Compos. Part A Appl. Sci. Manuf. 100 (2017) 215–226, https:// doi.org/10.1016/j.compositesa.2017.05.017.
- [38] A.K. Bledzki, A.A. Mamun, J. Volk, Physical, chemical and surface properties of wheat husk, rye husk and soft wood and their polypropylene composites, Compos. Part A Appl. Sci. Manuf. 41 (2010) 480–488, https://doi.org/10.1016/j. compositesa.2009.12.004.
- [39] Y. Peng, S.S. Nair, H. Chen, N. Yan, J. Cao, Effects of lignin content on mechanical and thermal properties of polypropylene composites reinforced with micro particles of spray dried cellulose nanofibrils, ACS Sustain. Chem. Eng. 6 (2018) 11078–11086, https://doi.org/10.1021/acssuschemeng.8b02544.
- [40] S. Ikram, O. Das, D. Bhattacharyya, A parametric study of mechanical and flammability properties of biochar reinforced polypropylene composites, Compos. Part A Appl. Sci. Manuf. 91 (2016) 177–188, https://doi.org/10.1016/j. compositesa.2016.10.010.
- [41] H.L. Tekinalp, X. Meng, Y. Lu, V. Kunc, L.J. Love, W.H. Peter, et al., High modulus biocomposites via additive manufacturing: cellulose nanofibril networks as "microsponges, Compos. Part B Eng. 173 (2019), 106817, https://doi.org/ 10.1016/j.compositesb.2019.05.028.
- [42] A. Alhelal, Z. Mohammed, S. Jeelani, V.K. Rangari, 3D printing of spent coffee ground derived biochar reinforced epoxy composites, J. Compos. Mater. (2021), https://doi.org/10.1177/00219983211002237.
- [43] Q. Zhang, H. Cai, W. Yi, H. Lei, H. Liu, W. Wang, et al., Biocomposites from organic solid wastes derived biochars: a review, Materials (Basel) 13 (2020) 1–16, https:// doi.org/10.3390/MA13183923.
- [44] H. Wang, B. Gao, J. Fang, Y.S. Ok, Y. Xue, K. Yang, et al., Engineered biochar derived from eggshell-treated biomass for removal of aqueous lead, Ecol. Eng. 121 (2018) 124–129, https://doi.org/10.1016/j.ecoleng.2017.06.029.
- [45] H. Lyu, B. Gao, F. He, A.R. Zimmerman, C. Ding, H. Huang, et al., Effects of ball milling on the physicochemical and sorptive properties of biochar: experimental observations and governing mechanisms, Environ. Pollut. 233 (2018) 54–63, https://doi.org/10.1016/j.envpol.2017.10.037.
- [46] Z. Mohammed, S. Jeelani, V. Rangari, Effect of low-temperature plasma treatment on surface modification of polycaprolactone pellets and thermal properties of extruded filaments, JOM 72 (2020) 1523–1532, https://doi.org/10.1007/s11837-020-04004-v
- [47] B. Sajjadi, W.Y. Chen, D.L. Mattern, N. Hammer, A. Dorris, Low-temperature acoustic-based activation of biochar for enhanced removal of heavy metals, J. Water Process Eng. 34 (2020), 101166, https://doi.org/10.1016/j. iwne.2020.101166.
- [48] S. Stankovich, D.A. Dikin, R.D. Piner, K.A. Kohlhaas, A. Kleinhammes, Y. Jia, et al., Synthesis of graphene-based nanosheets via chemical reduction of exfoliated graphite oxide, Carbon N. Y. 45 (2007) 1558–1565, https://doi.org/10.1016/j. carbon.2007.02.034.
- [49] R. Geyer, J.R. Jambeck, K.L. Law, Production, use, and fate of all plastics ever made, Sci. Adv. 3 (2017) 3–8, https://doi.org/10.1126/sciadv.1700782.
- [50] V.P. Ranjan, S. Goel, Recyclability of polypropylene after exposure to four different environmental conditions, Resour. Conserv. Recycl. 169 (2021), 105494, https://doi.org/10.1016/j.resconrec.2021.105494.
- [51] P.W. Huang, H.S. Peng, Number of times recycled and its effect on the recyclability, fluidity and tensile properties of polypropylene injection molded parts, Sustain (2021) 13, https://doi.org/10.3390/su131911085.
- [52] A.L. Woern, D.J. Byard, R.B. Oakley, M.J. Fiedler, S.L. Snabes, J.M. Pearce, Fused particle fabrication 3-D printing: recycled materials' optimization and mechanical properties, Materials (Basel) (2018) 11, https://doi.org/10.3390/ma11081413.
- [53] A.A. Alghyamah, A. Yagoub Elnour, H. Shaikh, S. Haider, A. Manjaly Poulose, S. M. Al-Zahrani, et al., Biochar/polypropylene composites: a study on the effect of pyrolysis temperature on crystallization kinetics, crystalline structure, and thermal stability, J. King Saud. Univ. Sci. 33 (2021), 101409, https://doi.org/10.1016/j. iksus.2021.101409.
- [54] J. Dlouhá, L. Suryanegara, H. Yano, The role of cellulose nanofibres in supercritical foaming of polylactic acid and their effect on the foam morphology, Soft Matter 8 (2012) 8704–8713, https://doi.org/10.1039/c2sm25909e.
- [55] L. Wang, J. Shen, Y. Men, Y. Wu, Q. Peng, X. Wang, et al., Corn starch-based graft copolymers prepared via ATRP at the molecular level, Polym. Chem. 6 (2015) 3480–3488, https://doi.org/10.1039/c5py00184f.
- [56] M. Idrees, S. Jeelani, V. Rangari, Three-Dimensional-printed sustainable biocharrecycled PET composites, ACS Sustain. Chem. Eng. 6 (2018) 13940–13948, https://doi.org/10.1021/acssuschemeng.8b02283.
- [57] M. Spoerk, C. Holzer, J. Gonzalez-Gutierrez, Material extrusion-based additive manufacturing of polypropylene: a review on how to improve dimensional inaccuracy and warpage, J. Appl. Polym. Sci. (2020) 137, https://doi.org/ 10.1002/app.48545.
- [58] S. Hertle, M. Drexler, D. Drummer, Additive Manufacturing of poly(propylene) by means of melt extrusion, Macromol. Mater. Eng. 301 (2016) 1482–1493, https://doi.org/10.1002/mame.201600259.
- [59] M. Spoerk, J. Gonzalez-Gutierrez, C. Lichal, H. Cajner, G.R. Berger, S. Schuschnigg, et al., Optimisation of the adhesion of polypropylene-based materials during extrusion-based additive manufacturing, Polymers (Basel) (2018) 10, https://doi.org/10.3390/polym10050490.